RSC Advances

ROYAL SOCIETY OF CHEMISTRY

www.rsc.org/advances

Unusual surface and solution behaviour of keratin polypeptides

Zhiming Lu[1], Fang Pan[1], Dong Wang[2], Mario Campana[1], Hai Xu[2], Ian M. Tucker[3], Jordan T. Petkov[3,4], John Webster[5], and Jian R. Lu[1]

[1] Biological Physics Laboratory, School of Physics and Astronomy, University of Manchester, Oxford Road, Manchester, M13 9PL, United Kingdom.

[2] Centre for Bioengineering and Biotechnology, China University of Petroleum (East China), Qingdao 266580, China

[3] Unilever Research and Development Laboratory, Port Sunlight, Quarry Road East, Bebington, Wirral CH63 2JW, United Kingdom

[4] Menara KLK 1, Jalan Pju 7/6, Mutiara Damansara, 47810 Petaling Jaya, Selangor Darul Ehsan, Malaysia

[5] ISIS Neutron Facility, Science and Technology Facilities Council, Rutherford Appleton Laboratory, Harwell Science and Innovation, Campus, Didcot OX11 0QX, United Kingdom

*Author to whom correspondence should be addressed. Email: j.lu@manchester.ac.uk

Abstract

Keratins are filament proteins, but we report in this work that water-soluble keratin polypeptides hydrolyzed from wool could readily adsorb onto the surface of water and could thus be used as surface active biomaterials. Neutron reflection measurements with the help of deuterium labelling were used to determine the adsorbed amount and distribution of the polypeptide layers formed. It was found that the interfacial layers were comprised of two main regions, a dense top layer of 18-25 Å and a loose bottom layer of 25-30 Å. Half of the top dense layer was exposed to air with the remainder of the top layer and the diffuse bottom layer immersed in the aqueous solution. Both the volume fraction and the layer thickness increased with keratin solution concentration as did the adsorbed amount which was seen to plateau just above 2 mg m^{-2} at approximately 0.1 g dm^{-3} (2.1μM). Increase in [NaCl] led to the reduced surface adsorption, accompanied with the thinning of the top layer. Cryo-TEM imaging revealed that the keratin aggregates had an ellipsoidal structure with radii ranging from 60 Å to 220 Å. The ellipsoidal shape was well supported by SANS, with the major radius of 140 Å and the minor radius of 60 Å. With increasing [NaCl], the ellipsoids became thinner but longer, a feature consistent with the observed trend from surface adsorbed layer. This aunusual behaviour could be explained by the electrostatic screening effect. As the salt concentration increased, the polypeptide chains became stiffer and more readily aligned, resulting in thinner layers and longer aggregates.

Introduction

Keratins are widely distributed in the skin, hair and nails and provide both epithelial and endothelial coverage of organs. They are a member of the family of fibrous structural proteins [1]. Most current studies have focused on the understanding of their roles in health and diseases. For example, their interactions with other types of proteins and peptides can implicate diseases such as rheumatoid arthritis [2]; studies of DNA sequence coding for keratins and their mutations have revealed their inductions of skin conditions and related diseases [3-5]. In contrast, extensive research has also been undertaken in other fields such as cosmetics, animal foods and textiles [6, 7], with many studies directly focusing on fibres or nails. As a multifunctional biomaterial, there is an increasing interest to explore keratins' use as scaffolds in tissue engineering and regenerative medicine. Recent studies have identified two fundamental roles of keratins: as a structural support and in metabolic processes, with important repercussions in tissue reconstruction, cell seeding and diffusion, implantable biomaterials [8].

Most known keratins belong to the type I and type II classes of currently recognized intermediate filament proteins, with their molecular weights spanning from 40 kDa to 70 kDa [9]. The type I keratins often have smaller sizes with molecular weights of 40 – 48 kDa and acidic isoelectric points, and the type II ones are larger with molecular weights of 59 – 62 kDa and neutral or slightly basic isoelectric points. Human hair or sheep wool contain examples of both these two classes which can be further divided into hard keratins (type Ia and IIa) and soft keratins (type Ib and IIb). Eight major hard keratins containing four type Ia (a1, a2, a3, a4) and four type IIa (b1, b2, b3, b4) have been identified in different species [10]. Common to many of the intermediate filament proteins is the highly conserved central alpha-helical domain, which is comprised of four coiled-coil segments and non-helical terminal domains of varying lengths and sequences [11]. The acidic and basic soft keratins first interact to form the basic heterodimers and they can then pair up to create tetramers and the polymerisation process goes on to create the final 100 Å filament structures [12]. It is widely thought that wool and hair share a similar process in keratin filament formation because of their closely related secondary structures.

Yu et al have undertaken amino acid sequence comparisons between a human type Ia keratin a3 and other four type Ia hair keratins, including two from sheep and two from mouse. The a3 hair keratin has 404 amino acids, a molecular weight of 45,914 Da and an isoelectric point of 5.6, in contrast to the number of amino acids of 412 and the molecular weight of 48,300 Da (including an acetyl group on its N-terminal) from a wool microfilament keratin 8c-1 [13] and a molecular

weight of 47,600 Da from another wool type I microfilament keratin [14]. The comparisons show predominant sequence homologies with a small frequency of variations.

Keratin adsorption from aqueous solution could implicate many technological applications, for example, in personal care. To study keratin adsorption at different interfaces, a stable keratin solution is required. An important feature of keratin as compared to other proteins such as collagen and elastin is the existence of a large number of disulphide bonds and hydrophobic amino acids. This makes it difficult to dissolve keratin in most solutions or solvents including water [15]. The keratin used in this work was extracted from sheep wool by utilising reducing agents to break the disulphide bonds. This produces keratin which is readily soluble in water. In this extraction process, the reducing agents cause little chemical alteration or damage to the protein[16]. Although keratins have previously been rendered water-soluble by a range of approaches, information regarding their adsorption at interfaces and aggregation in solution is required for their use in this field. Of current interest is also the investigation of their interactions with various formulation ingredients such as surfactants. The work reported here presents an initial study of the surface adsorption and solution aggregation of keratin derived from wool using a combination of surface tension measurements, neutron reflection (NR), dynamic light scattering (DLS) and small angle neutron scattering (SANS).

Protein folding and related structural changes in solution have been of interest over recent decades[17-19]. Due to difficulties in the measurement of their structural changes experimentally, a combination of techniques is usually required. Various types of nuclear magnetic resonance techniques including nuclear overhauser effect spectroscopy (NOSEY) have provided a wealth of information regarding intra- and inter-molecular structures with a high degree of resolution [20]. However, these methods have limitations on the detection of interfacially adsorbed protein layers, particularly at the air/liquid interface. Circular dichroism (CD) determines a protein's secondary structures by detecting the optical polarisation associated with the chiral centres under different environments [21]. Fourier transform infrared spectroscopy (FTIR) is also able to reveal secondary structural information at both substrate interface and solution. [22] Additional techniques including ellipsometry and dual polarisation interferometry (DPI) are capable of measuring the adsorbed amount of materials at an interface, but it is difficult for them to detect structural changes in the protein layers [22, 23].

Neutron reflection has been widely used in thin film studies and is one of the most commonly used techniques for the study of the adsorption of surfactants, polymers, proteins, and their

mixtures, at different interfaces [24, 25]. This technique, when used in conjunction with selective deuterium labelling[26], has the unique advantage of allowing for the determination of each individual component in a mixture. A further advantage of neutron reflection is that it allows measurement of both the adsorbed amount and the thickness of the adsorbed layer with Ångstrom resolution[27, 28]. Because NR is highly sensitive to the H/D isotopic substitution, simultaneous measurements can be performed by labelling the adsorbing species, or by using H_2O, D_2O or any of their mixtures to highlight the interface differently. This results in significant improvements in the sensitivity and resolution of the interfacial structures. Whereas NR at an air/water interface provides a useful tool in determining the structural conformations of keratin molecules at the interface, the scattering profile from SANS provides a way to estimate the dimensional conformations of the keratin molecules and possible formation of aggregates. The effect of salt in producing structural changes in the keratin molecules can also be investigated.

Materials and Methods

Materials

Keratin production

White sheep wool was purchased from Brunswick Industrial Estate, Halifax, West Yorkshire, UK in the spring of 2011. Keratin K1S sample was obtained by following a recognised procedure with the application of some modifications [29, 30]. The modification involved the immersion of 1 g of degreased wool (fine cuts) in 10 mL of the dissolving solution comprised of 8 M urea, 0.2 M SDS and 0.5 M $Na_2S_2O_5$. The mixture was then heated to 100 °C for a period of 30 min and filtered and washed through a stainless steel mesh. The filtered solution was then encased in cellulose tubing (molecular weight cut-off of 12000-14000 Da (Sigma)) at an ambient temperature of 18-20 °C for dialysis against distilled water. The water was replaced every 4~5 hours during dialysis for approximately 4 days in order to remove excess reagents (urea, SDS and $Na_2S_2O_5$), with the final conductance close to that of the pure water. The obtained keratin stock solution was stored at 4°C prior to subsequent use. Its concentration could be obtained by either UV absorption measurement or weighing the power after freeze drying a given amount of the stock.

Investigation of the molecular weight distribution of the extracted keratin was carried out by SDS polyacrylamide gel electrophoresis (SDS-PAGE), using the Mini-PROTEAN 3 Cell

system from Bio-Rad. Stacking gels (6% acrylamide of about 0.75 mm thickness) and resolving gels (12% acrylamide of about 0.75 mm thickness) were prepared according to a standard method described by the Mini-PROTEAN 3 Cell Instruction Manual (run at a constant voltage of 150 V). Keratins were visualized by Coomassie Brilliant blue G 250 stain using a protein marker (Biolabs) for calibration. The molecular weight distribution of extracted wool keratins was observed as two main bands, at approximately 45 kDa (equivalent to type Ia keratins) and 60 kDa (equivalent to type IIa keratins). In addition, several weak bands were observed, corresponding to the low molecular weights at approximately 6-9 kDa and 10-20 kDa, which were attributed to the high-sulphur and high-glycine/tyrosine proteins of the matrix and the low-sulphur intermediate filament proteins. These parameters obtained from the wool keratin extractions are consistent with the results reported previously by other groups[29, 30].

For ease of data analysis in neutron reflection, it is necessary to use one keratin as a model molecule for the estimate of its scattering length density (SLD) and calculation of the amount of surface adsorption. Table SI1 in Support Information shows how SLD values vary with the ratio of H_2O and D_2O due to the labile H/D exchanges. An important observation is that the SLD values change little for different proteins in a given solvent such as H_2O. This illustrates that although proteins differ in sequence and in their physical and biological properties, all their amino acid compositions tend to be similar [31].

Preparation of keratin solutions

The sample solutions of keratin used in this work were prepared with ultrapure water (Elga, Vivendi Water Systems Ltd.) containing 5 mM NaCl. Solution pH was adjusted to the required value by use of the minimum amount of HCl or NaOH. All measurements were carried out at an ambient temperature of approximately 25 $^{\circ}$C unless otherwise stated.

Methods

Surface Tension

Surface tension of keratin solutions was measured on a Kruss K100 using the Wilhelmy plate method, at a temperature of 25°C. Surface tension profiles showed a marked time-dependent changes, but in almost all cases surface tension tended to equilibration when measured up to 15000 s (about 4 hr).

Neutron Reflectivity

Specular neutron reflection determines the neutron refractive index (*n*) profile normal to an interface, and can be expressed as:

$$n(\lambda) \approx 1 - \frac{\lambda^2}{2\pi} Nb \quad (1)$$

where λ is the neutron wavelength, N is the atomic number density and b the coherent scattering length. Nb, commonly referred to as the scattering length density (SLD) or ρ, varies linearly with interfacial composition:

$$\rho = \sum_j \varphi_j \rho_j \quad (2)$$

φ_j and ρ_j are, respectively, the volume fraction and the scattering length density of each component. One important feature of neutron scattering is that hydrogen and deuterium have very different scattering lengths (b_H = -3.74×10^{-5} Å, b_D = 6.67×10^{-5} Å). The scattering length density can be manipulated by deuterium labelling. This approach has been extensively used in a number of surfactant [32] and protein [33] systems to obtain information about the adsorbed amount and interfacial composition. The same approach could be used to vary the SLD of the solvent to highlight the adsorbed layer differently.

Neutron reflectivity profiles are often analysed via the optical matrix method [34]. The interfacial region is modelled assuming a finite number of layers, each characterised by a certain thickness (τ_i) and scattering length density (ρ_i). The reflectivity is then calculated from the model and compared to the experimental data and the process is iterated until a good fit is obtained. If the adsorbed layer can be modelled by a one-layer fitting, the molecular volume fraction of the protein (φ_s) in the layer can be calculated from the following equation [35]:

$$\varphi_s = \frac{\rho - \rho_w}{\rho_s - \rho_w} \quad (3)$$

where ρ_s, ρ_w and ρ are the scattering length densities of keratin (1.91 × 10^{-6} Å^{-2} for keratin in H_2O, 3.40 × 10^{-6} Å^{-2} for keratin in D_2O), the solution (0 for NRW and 6.35 × 10^{-6} Å^{-2} for D_2O) and the total layer, respectively. The volume fraction of keratin adsorbed at the air/NRW

interface can be easily calculated by the ratio of ρ / ρ_s. The area per molecule (A) can then be obtained via;

$$V_s = A\tau\rho_s; \qquad (4)$$

where V_s is the volume of keratin molecule and τ is the thickness of the keratin layer. The adsorbed amount can then be expressed as:

$$\Gamma = \frac{MW}{6.023 \times A} \qquad (5)$$

MW is the molecular weight of keratin and in this case we referred to the sheep wool keratin [14]. The total volume of keratin was calculated by summing up the volume of all individual amino acids inside the molecule, giving a total of 56.6×10^3 Å^3 as shown in Table SI1.

The neutron reflection experiments were performed at the ISIS Neutron Facility, Rutherford Appleton Laboratory, Didcot, UK. The reflectometer SURF was used with a white neutron beam wavelength from 0.5 to 6.5 Å. Each reflectivity profile was combined from the measurements taken at three different incidence angles of 0.5°, 0.8° and 1.5°covering a momentum transfer (Q) from 0.015 to 0.5 Å^{-1}. The system was calibrated by measuring a pure D_2O profile in order to determine the scale factor. The typical background in null reflecting water (NRW) was 7×10^{-6} Å^{-2} and that in D_2O was 2×10^{-6} Å^{-2}. All NR measurements were performed with Teflon troughs in a carrier containing 5 troughs at a time. The neutron beam was defined by two sets of horizontal and vertical slits placed before the sample trough, providing a neutron beam with an illuminated area of some 10×3 cm^2.

Dynamic light scattering (DLS)

Dynamic light scattering (DLS) has been widely used as a convinient method to determine the average size of protein molecules in different conditions of bulk solution. The detailed principles of DLS as well as its applications are decribed by Berne *et al.* [36]. Basicly, all particles in the solution are illuminated with light of a specific wavelength and DLS measured the intensity fluctuations from the scattered light between 1 ns and 1 ms. In this work, all DLS measurements were performed using a Malvern Instrument Nanosizer. The instrument was fitted with a helium-neon laser (633 nm) with a size detection range from 6 Å to 6 μm. Six measurements were performed on each sample, with an average of 5 runs taken for each

measurement, each within 1 min. More information about DLS can be referred to from Support Information.

Small Angle Neutron Scattering

SANS is widely used for detecting both the size and shape of particles in solution such as aggregates of polymers, surfactants and biomaterials. It is able to probe structures at length scales from 10 Å to more than 1000 Å. The SANS in this work was used to detect the structures of keratin in bulk solution under different ionic strengths. More information about SANS theories and model fittings can be referred to from Support Information. In this work, the SANS experiments were performed on LOQ at ISIS Neutron Facility, Rutherford Appleton Laboratory, Didcot, UK. The neutrons provided had a wavelength range of 2.2-10 Å with a chopper to cut the overlapped area between two pulses of neutrons. The 64 cm square detector was at a distance of 4.1 m, giving a κ range of 0.006-0.28 Å^{-1}. Samples were contained in 2.0 mm pathlength fused silica cells. Data were corrected for the wavelength dependence of the incident spectrum, the measured sample transmission, and relative detector efficiencies, prior to subtraction of the respective D_2O buffer backgrounds. Absolute scaling was obtained by comparison with the scattering from a partially deuterated polystyrene standard. The data were fitted using the SASView program, developed through the work of several collaborators on the NSF DANSE project and provided by RAL.

### *Cryo-transmission electron microscopy*

The cryo-TEM samples were prepared in a controlled environment vitrification system (CEVS). ~4 μL sample solution was coated onto a TEM copper grid and the grid was blotted with two pieces of filter paper for about 2 seconds, leading to the formation of a solution thin film. Then, the grid was quickly plunged into a reservoir of liquid ethane (-165 ºC, cooled by liquid nitrogen) and then kept in liquid nitrogen until the observation. After transferring the grid to a cryogenic sample holder (Gatan 626) and putting the holder into a JEOL JEM-1400 Plus TEM (120KV) instrument at about -174 ºC, one could observe the nanostructures.

Results

(A) Surface Tension

Surface tension measurements were first carried out to outline the interfacial adsorption behaviour of the keratin solutions focusing on revealing their dynamic adsorption with time.

These surface tension studies also provide an estimate of the concentration range required in the subsequent neutron reflectivity work. Figure 1 shows the time dependent surface tension changes for a series of solutions prepared at pH 6. At the lowest concentration of 3×10^{-4} mg/ml, no surface tension reduction was observed over the entire measurement period. As the keratin concentration was increased to 1×10^{-3} mg/ml, there was an initial induction period of some 3000s, after which the surface tension showed a clear trend of decline. With further increase in keratin concentration, this induction period was seen to reduce, with the interfacial adsorption accelerating. As the keratin concentration was increased up to 0.1 mg/ml, there was a further reduction of the induction time (Figure 1b). Further increase in keratin concentration above that point was seen to produce relatively small changes in the surface tension profile, indicating the saturation of interfacial adsorption. On the basis of these and other surface tension measurements (not presented here), a concentration of 0.1 mg/ml was taken to be the approximate concentration around which the saturated keratin adsorption could be reached under these experimental conditions.
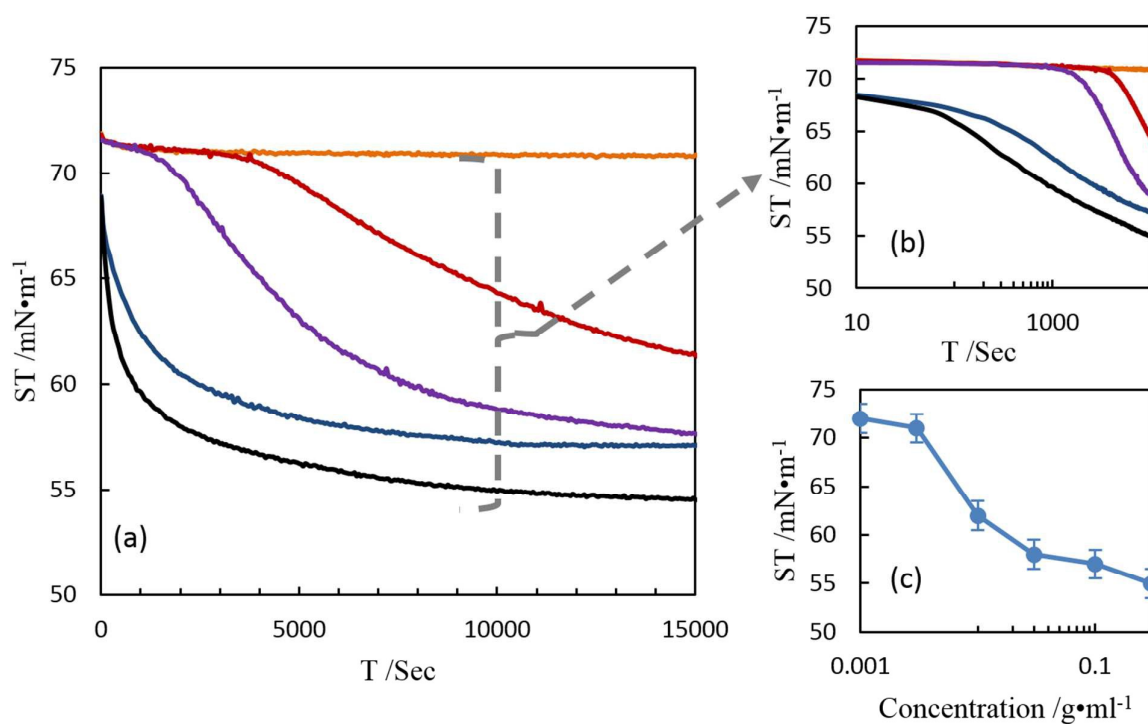
Figure 1 Surface tension measured over time from keratin solutions at pH 6. From top to bottom, concentrations were fixed at 3×10^{-4} mg/ml, 1×10^{-3} mg/ml (0.21 μM), 3×10^{-2} mg/ml, 0.1 mg/ml and 0.3 mg/ml (6.3 μM). (a) Linear plots; (b) Logarithmic plots highlight the concentration-dependent lag time for interfacial adsorption; (c) equilibrium surface tension as a function of keratin concentrations.

(B) Neutron Reflectivity

(B1)   Reflectivity profiles of keratin in NRW subphase

Neutron reflectivity was initially used to determine the adsorbed amount of keratin at the air/water interface as a function of increasing protein concentration. This is usually carried out using a mixture of approximately 8% D_2O in H_2O, termed null-reflecting water (NRW). NRW has the same scattering length density as air, and hence all reflectivity signal at this interface originates from the adsorbed interfacial layer. The measurements under this contrast can provide invaluable information regarding both adsorbed amount and interfacial thickness without any interference from water across the interface [35, 37]. Reflectivity profiles for a series of keratin solutions ranging from 3×10^{-3} to 0.3 mg/ml at 25˚C, pH 6 and 5 mM NaCl are shown in Figure 2(a), where reflectivity R is plotted against wave vector Q. The reflectivity can be seen to increase with increasing keratin concentration, and then to reach almost full adsorption at a concentration of 0.1 mg/ml, followed by small changes when the concentration was further increased to 0.3 mg/ml. It should be noted that time dependent effects were avoided in these NR measurements by ensuring that after the solutions had been loaded into the liquid troughs, a state of equilibrium was reached, with the timescales referred to from the surface tension data shown in Figure 1.
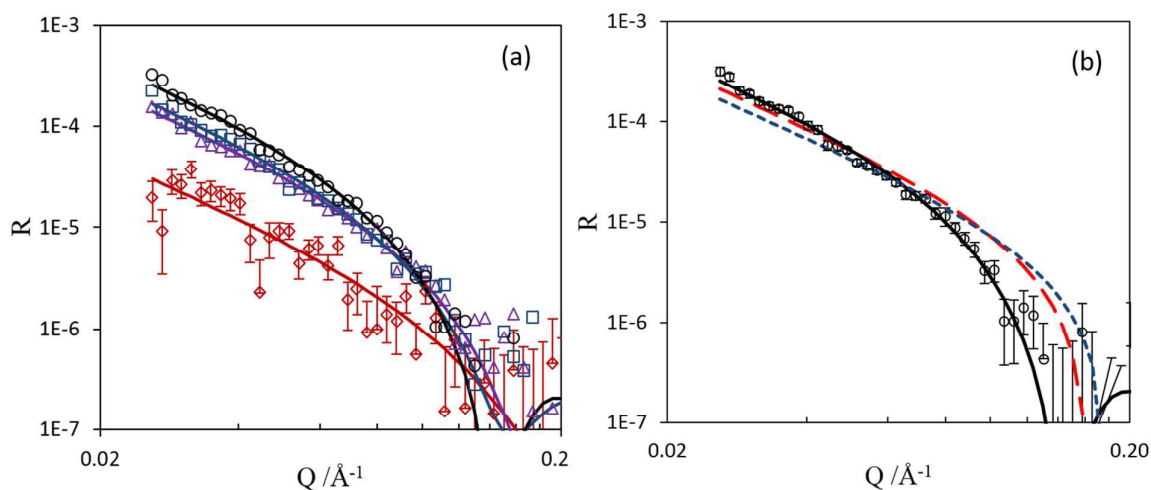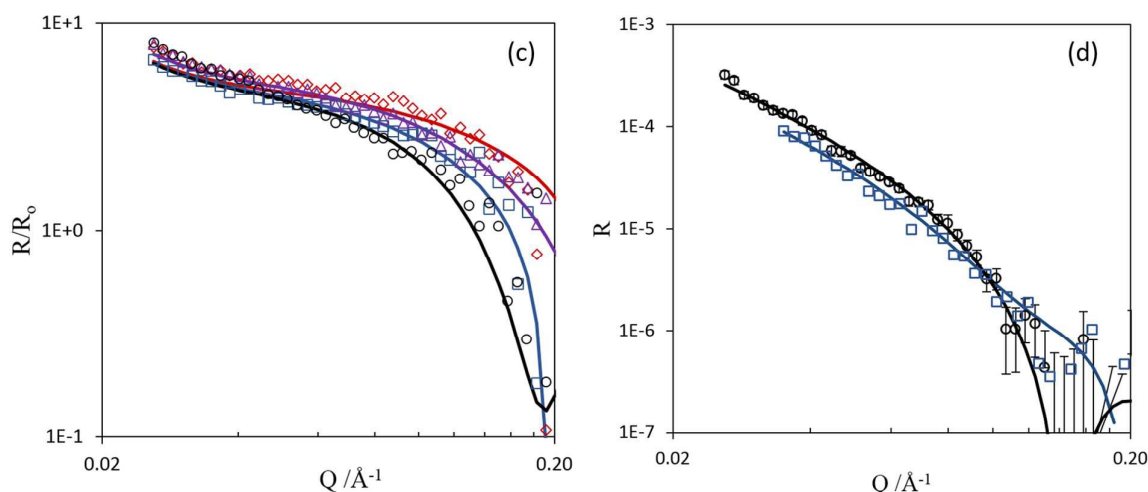
Figure 2 Neutron reflectivity (R) measured at the air/NRW interface. (a): The adsorption of keratin at 0.003 (◊), 0.01 (□), 0.03 (Δ) and 0.3 (o) mg/ml, with NaCl concentrations kept at 5mM; (b): the adsorption of keratin at 0.1 mg/ml. The red dashed line indicates the best uniform layer fit with a thickness of 30 Å and a volume fraction of the protein at 0.6. The green dotted line also shows a uniform layer fit with a thickness of 25 Å and a volume fraction of protein also at 0.6. The continuous line represents the best fit of a two layer model with a top dense layer of 25 Å on the air side and a bottom dilute layer of 30 Å in NRW. The solid lines indicate the optimum two layer fits; (c): NR profiles plotted in the form of R/Ro (where Ro denotes reflectivity from the sharp air/D_2O interface) measured from keratin adsorption onto the D_2O surface at concentrations of 3×10^{-3}(◊), 1×10^{-2} (□), 3×10^{-2} (Δ), 0.3 (o) mg/ml in 5 mM NaCl. Solid lines indicate the best fits to the data measured. The original reflectivity profiles are shown in Figure SI4. (d): the adsorption of keratin at 0.3 mg/ml in NRW in 5 mM NaCl (o) and in 500 mM NaCl (□). The lines indicate the best fits to the data: the thickness of the dense top layer reduces from 25 Å to 19 Å with NaCl being increased from 5 mM to 500 mM. All measurements were performed under a temperature of 25 °C at pH 6.7±0.1.

An initial fit to the profiles using a one layer fit proved unsatisfactory. An example of this can be seen in the reflectivity profile for 0.1 mg/ml as shown in Figure 2(b). It can be seen that the red (long dashed) line and green (short dashed) line, both of which represent the best one layer fits to the measured profile, and fail to adequately model the data. Introduction of a second layer in the interfacial region with a lower scattering length density produced an improved fit to the data as shown by the continuous line in Figure 2(b).

Table 1 The best two layer model fits to reflectivity profiles shown in Figure 2(a) under different keratin concentrations in NRW. NaCl concentration is 5 mM, at 25 °C. NRW is null reflecting water.

[Keratin] mg/ml	Layer	Thickness (Å) ±1	SLD (×10⁻⁶ Å⁻²) ±0.02	Volume fraction ±0.02	Layer mass (mg/m²) ±0.03	Total mass (mg/m²) ±0.04

0.003	1	18	0.6	0.30	0.75	0.88
	2	20	0.11	0.05	0.13	
0.01	1	22	1	0.50	1.53	1.81
	2	24	0.16	0.08	0.28	
0.03	1	24	1.06	0.53	1.76	2.06
	2	26	0.17	0.08	0.30	
0.1	1	25	1.1	0.55	1.90	2.29
	2	26	0.22	0.11	0.39	
0.3	1	25	1.1	0.55	1.90	2.29
	2	26	0.22	0.11	0.39	

The adsorbed interfacial layers were therefore modelled by a dense top layer with thickness increasing from 18 to 25 Å covering a concentration ranging from 0.003 to 0.01 mg/ml. The corresponding second layers were much looser, extending towards the bulk aqueous phase with a layer thickness in the increasing order ranging from 18 to 26 Å over the same concentration range. The volume fraction of keratin in both the top and bottom layers increased with increasing concentrations, ranging from 0.3 to 0.6 for the dense top layer and 0.05 to 0.11 for the loose bottom layer. The adsorbed amount of keratin increased with increasing protein concentration and reached the highest value of 2.29 mg/m^2 at a concentration of 0.1 mg/ml. Little further increase was observed at the highest concentration of 0.3 mg/ml studied. Figure 2(a) shows the NR profiles at the air/NRW interface with the 4 representative keratin concentrations studied and the continuous lines denote the best 2 layers following the structural features as outlined for the reflectivity data measured at 0.1 mg/ml with due adjustments of layer thickness and composition depending on the keratin concentration concerned, with the best fitted parameters shown in Table 1.

(B2)   Reflectivity profiles of keratin in the D_2O subphase

Reflectivity profiles measured at the air/D_2O interface from keratin solutions prepared in D_2O are shown in Figure 2(c). The use of D_2O as the subphase allows more insight to be gained regarding the interfacially adsorbed structure of keratin. D_2O possesses a very different SLD from air, and thus the reflectivity profiles shown in Figure 2(c) contain contributions from the adsorbed keratin layer, the D_2O subphase and interferences between them. This allows information to be obtained regarding the proportions of keratin in air and in D_2O. The change in SLD for keratin upon moving from NRW to D_2O (2.03×10^{-6} Å^{-2} in NRW to 3.40×10^{-6} Å^{-2} in D_2O) has been taken into account.

In order to reduce the number of fitting parameters involved, the reflectivity profiles were modelled using the layer thickness and adsorbed keratin amount as determined from the corresponding NRW measurements, with the only variable being the extent of the top layer immersion into D_2O. The data indicate that the proportion of keratin immersed in the aqueous phase is much greater than that in air. As a result, it was necessary to split the top layer as fitted from the NRW into two separate layers, representing the fraction exposed to air and that immersed in water. The overall interfacial region was therefore described by a three layer model, in which the top layer is exposed to air and the remaining 2 layers are fully immersed into the aqueous phase. The layer exposed to air was found to increase in thickness from 10 to 13 Å as the concentration increased from 3×10^{-3} mg/ml to 0.03 mg/ml. No further increase was found as the concentration then increased to 0.3 mg/ml. For all concentrations studied, approximately half of the top layer was exposed to air and it contained approximately half of the total adsorbed mass. The fitting parameters used are listed in Table 2.

**Table 2** Three layer model fits to the reflectivity profiles of keratin measured in D_2O aqueous subphase.

[Keratin] mg/ml	Layer	Thickness (Å) ±1	SLD (×10⁻⁶ Å⁻²) ±0.02	Volume fraction ±0.02	Layer mass (mg/m²) ±0.03	Total Mass (mg/m²) ±0.04
0.003	1	10	1.1	0.3	0.42	0.92
	2	8	5.2	0.3	0.33	
	3	25	6.15	0.05	0.17	
0.01	1	12	1.6	0.47	0.78	1.63
	2	10	4.8	0.49	0.68	
	3	25	6.1	0.06	0.17	
0.03	1	13	1.8	0.53	0.96	2.08
	2	12	4.75	0.57	0.95	
	3	25	6.1	0.06	0.17	
0.1	1	13	1.9	0.56	1.02	2.25
	2	12	4.75	0.57	0.95	
	3	30	6.1	0.07	0.29	
0.3	1	13	1.9	0.56	1.02	2.25
	2	12	4.75	0.57	0.95	
	3	30	6.1	0.07	0.29	

(B3)   Reflectivity profiles of keratin with 0.5 M NaCl in the NRW subphase

In order to investigate the effect of electrolytes on the adsorption of keratin at the air/water interface, NR measurements in NRW were replicated in the presence of 500 mM NaCl. Table SI2 lists the best fitted parameters from the reflectivity profiles measured from the adsorbed surfaces of 0.3 mg/ml of keratin in 5 mM NaCl (illustrated by black circles) and 500 mM NaCl (illustrated by blue squares) as shown in Figure 2d. The decrease in reflectivity indicates a lower adsorbed amount as the salt concentration was increased. The thickness of the top dense layer was also found to decrease from 25 Å to 19 Å with increasing salt concentration, whereas the keratin volume fraction was little changed. The thickness of the bottom layer and the SLDs of both the top and bottom layers changed slightly. Therefore, it can be concluded that the reduced adsorption was directly linked to the loss of the polypeptides exposed to the air, which suggests that the keratin polypeptides may become more hydrophilic as a result of increased ion binding.

(C) Dynamic light scattering (DLS)

Figure 3 compares the hydrodynamic diameters of nanoobjects measured from keratin solutions in 1 mg/ml solution for different salt concentrations from DLS measurements. It can be seen that the size of these aggregates increased from 140 Å to 300 Å upon increase in the salt concentration from 5 mM to 0.5 M. The trend and size range detected are in broad agreement with the SANS results. The volume intensity of DLS is proportional to the total number of aggreates and their individual volumes. It can be seen from Figure 3 that the keratin solution with 5mM NaCl had the highest percentage of volume at its specific size dimension and was least polydisperse in their sizes. As salt concentration increased, the intensity declined and their size distribution became broader.
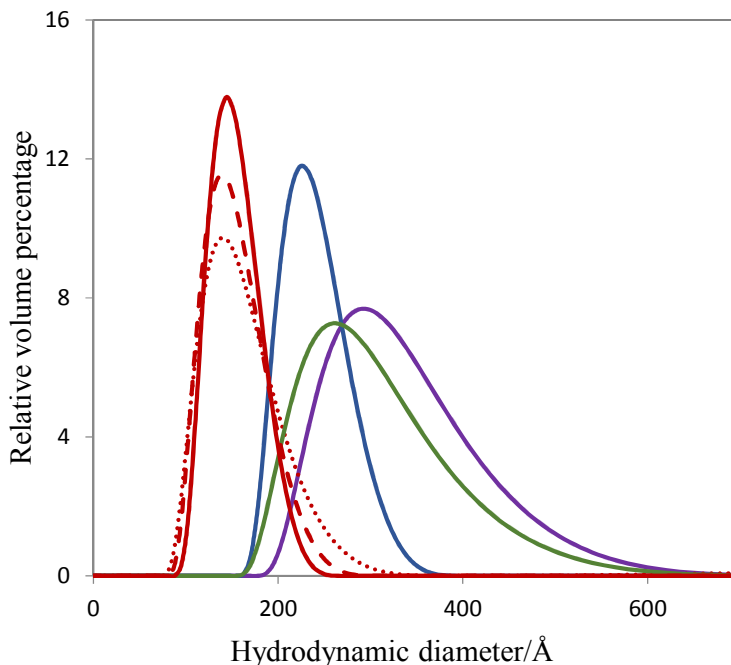
Figure 3 DLS size distribution of keratin polypeptides in 1 mg/ml solution with salt concentrations at 5 mM (red line), 100 mM (blue line), 200 mM (green line) and 500 mM (purple line), respectively. The dashed line and dotted line represented keratin solutions of 0.3 mg/ml and 0.1 mg/ml with 5 mM NaCl, respectively.

It is difficult to determine the sizes of the keratin solutions over the concentrations around 0.1 mg/ml, especially when their sizes vary in the range of 10 to 100 Å. In spite of this limitation, however, a set of DLS measurements was still performed from 0.01 mg/ml to 0.3 over 10 concentrations in total. The results (not shown here) indicated that the keratin solution must reach its critical aggregation concentration (CAC) at the concentration below 0.1 mg/ml, consistent with the trend observed from the surface tension measurements. Taken together, the DLS measurements depict progressive changes in the size and distribution of the keratin aggregates with increasing salt concentration, but at the lowest salt concentration the size distribution did not change much with keratin polypeptide concentration.

(D) Cryo-electron microscopy (cryo-EM) imaging
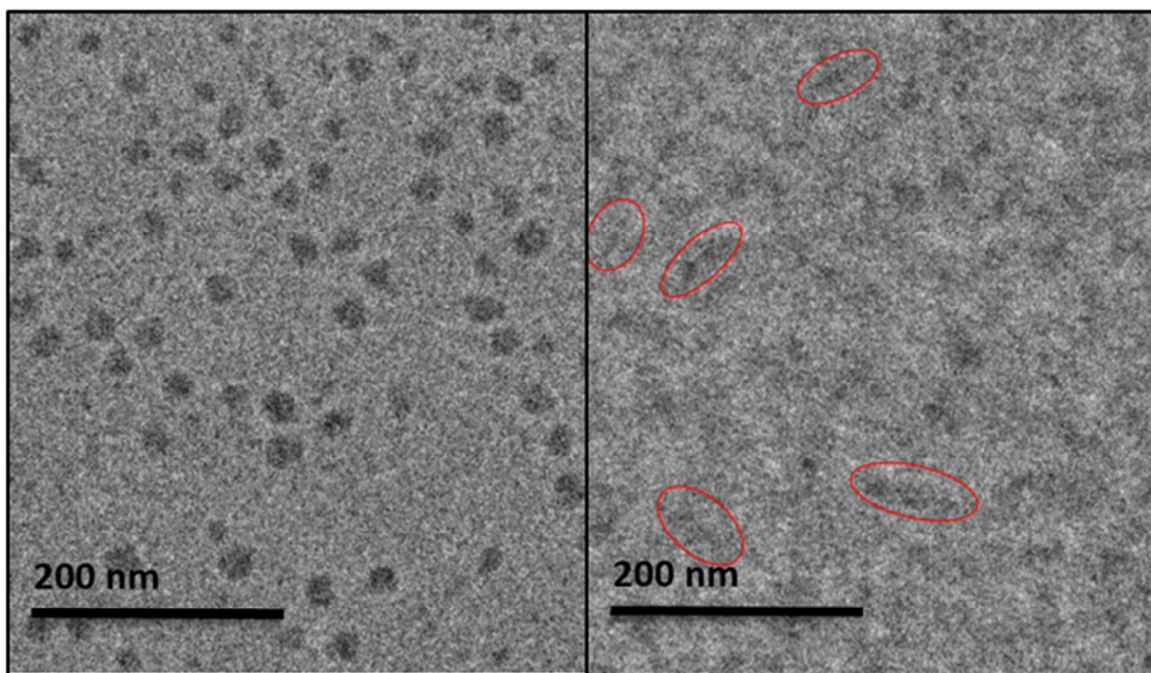
Figure 4 Unstained, frozen-hydrated keratin polypeptide solutions at 1 mg/ml and in 5 mM NaCl (left) and 500 mM NaCl (right) were imaged by Cryo-TEM. The dark regions represent keratin aggregates, contrasted against the background of vitreous ice, showing the elongation of the ellipsoidal aggregates with increasing salt concentration. Full images of cryo-EM are shown in Figure SI2 and SI3 in Support Information.

Cryo-transmission electron microscopy is an advanced microscopic technique to take high resolution images at the liquid nitrogen temperature of -174 ^{o}C. As the cryo-TEM samples were fast frozen, the aggregate structures were kept in almost native environment. No staining was required for imaging. Thus possible dehydration of the samples during observation could be avoided. The left image in Figure 4 shows the aggregates formed at 1 mg/ml keratin in 5 mM NaCl solution, showing ellipsoidal shape with radii ranging from 60 Å to 220 Å. In comparison, the keratin polypeptides in 500 mM NaCl solution (right image in Figure 4) formed thinner but longer structures.

(E) Small angle neutron scattering (SANS)

17
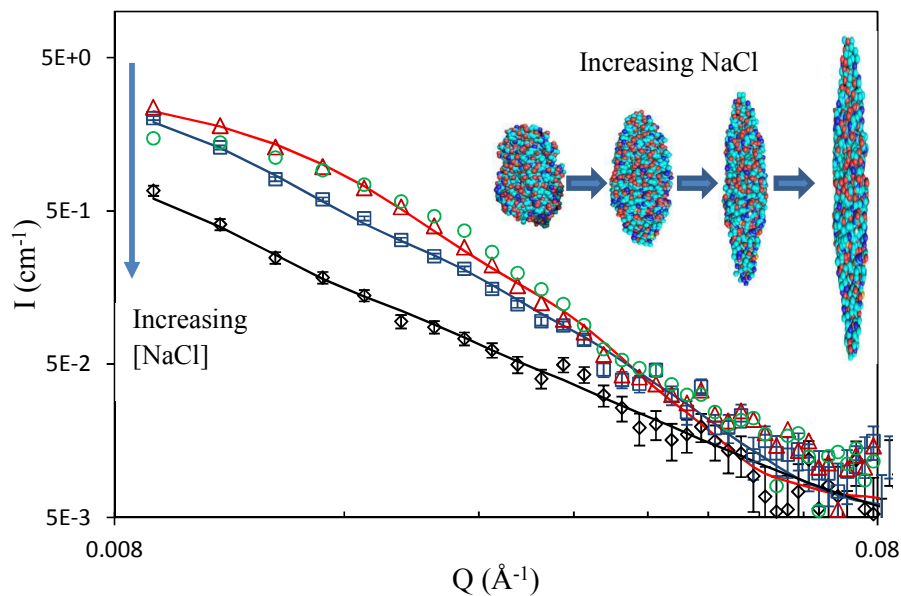
Figure 5 Neutron scattering intensity (I) plotted versus Q Effect of [NaCl] on keratin solution aggregation measured by SANS scattering with NaCl varied from 10 mM (O), 40 mM (Δ), 200 mM (□) to 500 mM (◊) at pH 6 in D_2O. The inset shows a schematic representation of the transition of the ellipsoidal shape with increasing NaCl concentration. A schematic representation of a steady shape change of keratin aggregates with increasing NaCl was embedded.

Figure SI5 in Support Information shows the scattering intensity profiles of keratin solutions with keratin concentration increasing from 0.25 mg/ml to 1 mg/ml. The intensity profiles from the three concentrations of keratin were different, but they remained the same shape, indicating that the size and shape of the scattering objects were the same. The best fitted parameters as shown in Table SI3 revealed that the aggregates were ellipsoidal with a long radius of 138±8 Å and a short radius of 59±2 Å. The fits are very sensitive to the short radius of the ellipsoid and less to the long radius. The only difference in the parameters fitted for the scattering profiles measured at the three concentrations was found to be the volume fraction. This implies that the polypeptides start to aggregate below 0.25 mg/ml and that change in the keratin concentration over this range did not alter the size and shape of the aggregates.

Figure 5 shows the scattering profiles of keratin solutions at 1 mg/ml of keratin concentration but with NaCl concentrations changing from 5 mM to 0.5 M in D_2O. It can be seen that increase in salt concentration reduced the scattered intensity gradually, suggesting that the size and shape of the ellipsoidal particles did change with increasing NaCl concentration. Specifically, the scattering profiles changed little over the low NaCl range, with larger reductions in scattering seen when [NaCl] was above 100 mM. The presence of NaCl in protein solution squeezed the

ellipsoidal particles, making them thinner and longer with increasing NaCl concentration. The short axial radius remained almost constant up to 100 mM NaCl. Above this concentration, the short axial radius began to decrease. The long axial radius showed a steady increase over the entire salt concentration range studied. In the presence of 500 mM NaCl, the keratin molecules became elongated with a short radius of 36 Å and a long radius of 306 Å, compared to the radii of 58 and 138 Å at 5 mM NaCl. The volume of the keratin aggregates can be calculated using

$$V = \frac{4}{3}\pi a^2 b \qquad (6)$$

where a and b are the short and long radii of the ellipsoid, respectively. The percentage of keratin in each aggregate can also be calculated as

$$P_{keratin} = \frac{\rho_{D_2O} - \rho_{aggre}}{\rho_{D_2O} - \rho_{keratin}} \qquad (7)$$

The volumes of the scattered particles under different NaCl concentrations were calculated using equation 6 and the results are listed in Table SI4. Whilst the aggregate shape showed a steady transition with NaCl concentration, the volume peaked around 100 mM NaCl. The volume fractions of keratin in keratin aggregates occupied an almost constant value of 0.6, except at the highest salt concentration of 500 mM, where it reduced to 0.4. Given that the molecular volume of keratin was taken to be approximately 56600 Å^3, the molecular number of keratin in an aggregate can be calculated. Over the entire salt concentration range studied, the average number of keratin molecules per micellar aggregate began at 21 at NaCl = 5 mM, peaked at 38 at NaCl = 100 mM and then reduced to 14 at NaCl = 500 mM.

These size and shape changes are also evident from the cryo-EM images shown in Figure 4. The ellipsoidal model is very sensitive to the short radius and the errors can be controlled well within ±2 Å. In contrast, the long radius has much less sensitivity, hence the fittings within ±10 Å being acceptable. The values of radius b listed in Table SI4 are the minimum values that could produce acceptable fits. Despite these uncertainties, the size and shape transitions as observed must be valid. The geometrical shape changes in the aggregates were also well supported by the DLS data as shown in Figure 3, where the measured hydrodynamic diameters of the aggregates show substantial variations in the peak values of aggregate size and size distribution.

Discussion

On the basis of SDS-PAGE analysis, the keratin polypeptide sample is comprised of hard keratins (Ia and IIa) with two main MW bands around 45 and 62 kDa. Although the polypeptides are able to adsorb and reduce surface tension over a wide concentration range, the extent of surface tension reduction is low, with the lowest surface tension of 55 mN/m being reached at 0.3 mg/ml (Figure 1c). The surface tension after 4 hours showed a steady decline with no clear occurrence of a break point to indicate the start of solution aggregation. DLS and SANS measurements confirmed the formation of aggregates at keratin polypeptide concentrations around 0.1 mg/ml, which was marked by the large hydrodynamic diameters peaked at approximately 144 Å (Figure 3) and ellipsoids with long axial lengths of approximately 138 Å from SANS (Figure SI5, Table SI3). At lower peptide concentrations, it was difficult to detect aggregation by SANS, but DLS showed clear signs of aggregates forming as the polypeptide concentration were reduced to 0.03-0.1 mg/ml, indicating that although the polypeptides were made soluble in the aqueous phase, they were highly prone to aggregation.

The NR work carried out explored both the concentration and salt effects of keratin adsorption at the air/water interface, with NRW and D_2O contrasts to highlight the layer structure and composition and their extent of immersion in water. All of the reflectivity profiles measured under different conditions revealed a two layer structure for the adsorbed keratin polypeptides: a top dense layer of 18-25 Å with a keratin volume fraction of 0.3-0.55 and a bottom loose layer of 25-30 Å with a keratin volume fraction of 0.05-0.11. The top layer was found to contain 80-85% of the polypeptides with the bottom layer containing the remaining 15-20%. The parallel measurements in D_2O revealed that almost half of the top layer was exposed to air and that this exposed region also contained almost half of the adsorbed polypeptides. Figure SI6 shows the total surface adsorbed amount as a function of keratin concentration. It can be seen that the adsorption plateaued upon approaching 0.1 mg/ml, which is consistent with the detection of aggregation by both DLS and SANS measurements around this concentration.

It is also evident from Figure 2(d) that increase in salt concentration caused reduction in the surface adsorption. However, the main part that contributed to the reduction of the adsorbed amount was the top dense layer, whereas the bottom loose layer remained broadly the same. The loss of the adsorbed polypeptides on the air side implied that the addition of salt caused them to become more hydrophilic, possibly through charge association or binding. However, the basic feature of a dense top layer and a loose bottom layer still remained. This feature of adsorbed protein layers has also been observed using human lactoferrin[38] and human serum albumin

(HSA) and bovine serum albumin (BSA) by NR [24], although it was thought that the adsorption of the albumins did not lead to any major structural unfolding.

The effect of salt concentration on the aggregation of keratin polypeptides was then studied by DLS. At the low NaCl concentration of 5 mM the hydrodynamic diameters were peaked around 200 Å. Increases in salt concentration above 100 mM led to the average diameters centering around 300 Å. The SANS work revealed an ellipsoidal shape of the aggregates with a short radius of approximately 60 Å and a long radius of approximately 140 Å under 5 mM NaCl. Increase in the ionic strength of the keratin solution was found to change the radii of the ellipsoids formed. It was found that the keratin molecules were stretched into thinner, longer ellipsoid shape with increasing salt concentration.

These size and shape changes of the aggregates appear to be highly unusual, but the trend is broadly consistent with the thinning of the adsorbed layers. Thus, the SANS and NR results were broadly consistent in that the addition of salt made the polypeptides stiffer, resulting in the formation of thinner layers and thinner but longer aggregates. The reduced aggregate size and adsorbed amount might also imply that the polypeptides became more hydrophilic.

The effects of ions on the conformation of polyelectrolytes has been explored quite extensively[39]. With reference to the interfacial adsorption and formation of films of synthetic polyelectrolytes by McAloney *et al.*[40] and Dubas *et al*[41], we can explain the observations as described in the work by electrostatic screening. The differences between the adsorbed layers and size and shape transitions of micellar aggregates formed under different salt concentrations could be accounted for by considering a conformational transition in the bulk polyelectrolyte solution, leading to a changed effective persistence length and chain stiffening. Unlike synthetic polymers, however, the keratin polypeptides used in this work contained several polypeptide chains, each bearing both positively and negatively charged amino acid groups. These oppositely charged groups could well work to promote the binding and association between neighbouring polypeptide chains, leading to the ion concentration induced transitions similar to the film features as observed by McAloney *et al.*[40] Figure 6 provides a schematic representation of the surface adsorbed layer and solution aggregation. It also depicts how the main features of surface adsorbed layers and solution aggregates formed change in response to the salt concentration increase.
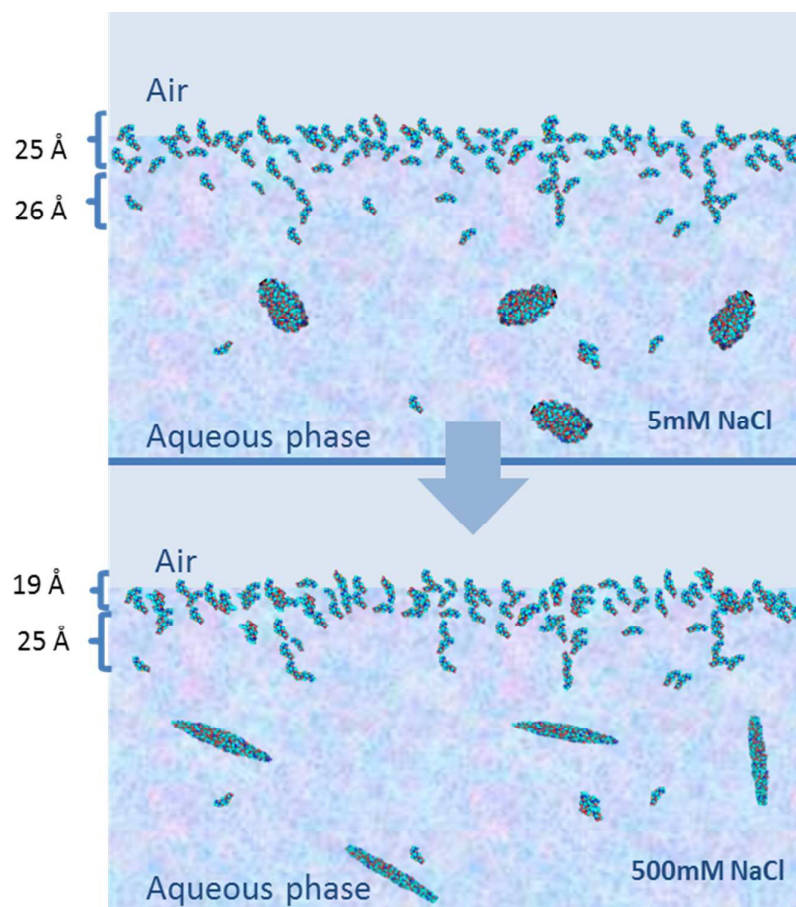
Figure 6 Schematic diagrams to show changes of the keratin distributions at the air/water interface and in bulk solution when the salt concentration was increased from 5 to 500 mM.

Conclusion

The keratins extracted from wool represent a renewable surface active biomaterial, attractive for a wide range of applications including skin care. Although water soluble up to relatively high concentrations, they can be readily adsorbed and aggregated. Surface adsorption was found to increase steadily and plateau at approximately 0.1 gdm^{-3}, around which solution aggregation also occurred. Although surface tension exhibited only a modest decline, neutron reflection revealed a substantial amount of keratin polypeptide adsorption over very low bulk concentration range over which the surface tension was high. The adsorbed keratin polypeptides formed a two-layer structure with a dense top layer of 18-25 Å and a loose bottom layer of 25-30 Å. The keratin occupied approximately 55% of the dense top layer at solution concentrations above 0.03 gdm^{-3} and 6-11% of the loose layer. Parallel D$_2$O measurements found that half of the dense top layer is exposed to air, highlighting the strong amphiphilic nature of the keratin

molecules. The SANS measurements found that the keratin aggregates adopted an ellipsoidal shape with a major radius of approximately 140 Å and a minor radius of approximately 60 Å in the low NaCl concentration of 5 mM, consistent with the DLS and cryo-EM measurements. Increase in NaCl was found to increase ion binding and chain stiffening, resulted in reduced adsorption and the thinning of the adsorbed layers, consistent with the stretching of the ellipsoidal aggregates formed in the bulk solution. These observed changes in surface adsorption and solution aggregation upon salt addition can be accounted for by the conformational transition of keratin aggregates from globular to ellipsoidal shape with salt concentration increasing, associated with polypeptide chain stiffening driven by electrostatic screening. This work has thus provided highly valuable information for developing the novel use of water soluble keratin polypeptides exploiting their unusual features of surface adsorption and solution aggregation.

References

1. D. Dhouailly, C. Xu, M. Manabe, A. Schermer and T.-T. Sun, *Experimental Cell Research*, 1989, **181**, 141-158.
2. P. Birkenfeld, N. Haratz, G. Klein and D. Sulitzeanu, *Clinical Immunology and Immunopathology*, 1990, **54**, 14-25.
3. N.-O. Ku, J. M. Darling, S. M. Krams, C. O. Esquivel, E. B. Keeffe, R. K. Sibley, Y. M. Lee, T. L. Wright and M. B. Omary, *Proceedings of the National Academy of Sciences*, 2003, **100**, 6063-6068.
4. Y.-N. Wang and W.-C. Chang, *Journal of Biological Chemistry*, 2003, **278**, 45848-45857.
5. R. C. Betz, L. Planko, S. Eigelshoven, S. Hanneken, S. M. Pasternack, H. Büssow, K. Van Den Bogaert, J. Wenzel, M. Braun-Falco and A. Rütten, *The American Journal of Human Genetics*, 2006, **78**, 510-519.
6. J. M. Cardamone, *Journal of Molecular Structure*, 2010, **969**, 97-105.
7. G. Secchi, *Clinics in Dermatology*, 2008, **26**, 321-325.
8. A. K. Smiley, J. M. Klingenberg, S. T. Boyce and D. M. Supp, *Burns*, 2006, **32**, 135-138.
9. J. F. Conway and D. A. Parry, *International Journal of Biological Macromolecules*, 1988, **10**, 79-98.
10. H. W. Heid, E. Werner and W. W. Franke, *Differentiation*, 1986, **32**, 101-119.
11. P. M. Steinert, A. C. Steven and D. R. Roop, *Cell*, 1985, **42**, 411-419.
12. P. Steinert and D. Roop, *Annual Review of Biochemistry*, 1988, **57**, 593-625.
13. L. M. Dowling, W. G. Crewther and A. S. Inglis, *Biochem. J*, 1986, **236**, 695-703.
14. J. Yu, D.-W. Yu, D. M. Checkla, I. M. Freedberg and A. P. Bertolino, *Journal of Investigative Dermatology*, 1993, **101**, 56S-59S.
15. P. M. Schrooyen, P. J. Dijkstra, R. C. Oberthür, A. Bantjes and J. Feijen, *Journal of Colloid and Interface Science*, 2001, **240**, 30-39.
16. A. Gupta, N. B. Kamarudin, C. Y. G. Kee and R. B. M. Yunus, *Journal of Chemistry and Chemical Engineering*, 2012, **6**, 732-737.
17. P. Privalov and N. Khechinashvili, *Journal of Molecular Biology*, 1974, **86**, 665-684.
18. G. M. Clore, A. T. Brünger, M. Karplus and A. M. Gronenborn, *Journal of Molecular Biology*, 1986, **191**, 523-551.

19.   A. Roy, A. Kucukural and Y. Zhang, *Nature Protocols*, 2010, **5**, 725-738.
20.   H. Roder, G. A. Elöve and S. W. Englander, *Nature*, 1988, **335**, 700.
21.   N. Sreerama and R. W. Woody, *Analytical Biochemistry*, 2000, **287**, 252-260.
22.   J. Armstrong, H. J. Salacinski, Q. Mu, A. M. Seifalian, L. Peel, N. Freeman, C. M. Holt and J. R. Lu, *Journal of Physics: Condensed Matter*, 2004, **16**, S2483.
23.   B. J. Cowsill, T. A. Waigh, S. Eapen, R. Davies and J. R. Lu, *Soft Matter*, 2012, **8**, 9847-9854.
24.   J. Lu, T. Su and R. Thomas, *Journal of Colloid and Interface Science*, 1999, **213**, 426-437.
25.   D. Lyttle, J. Lu, T. Su, R. Thomas and J. Penfold, *Langmuir*, 1995, **11**, 1001-1008.
26.   D. Cooke, C. Dong, J. Lu, R. Thomas, E. Simister and J. Penfold, *The Journal of Physical Chemistry B*, 1998, **102**, 4912-4917.
27.   I. Purcell, J. Lu, R. Thomas, A. Howe and J. Penfold, *Langmuir*, 1998, **14**, 1637-1645.
28.   J. Lu, *Annu. Rep. Prog. Chem., Sect. C: Phys. Chem.*, 1999, **95**, 3-46.
29.   C. Tonin, M. Zoccola, A. Aluigi, A. Varesano, A. Montarsolo, C. Vineis and F. Zimbardi, *Biomacromolecules*, 2006, **7**, 3499-3504.
30.   A. Vasconcelos, G. Freddi and A. Cavaco-Paulo, *Biomacromolecules*, 2008, **9**, 1299-1305.
31.   A. Cooper, M. W. Kennedy, R. I. Fleming, E. H. Wilson, H. Videler, D. L. Wokosin, T.-j. Su, R. J. Green and J. R. Lu, *Biophysical journal*, 2005, **88**, 2114-2125.
32.   J. Lu, R. Thomas and J. Penfold, *Advances in Colloid and Interface Science*, 2000, **84**, 143-304.
33.   X. Zhao, F. Pan and J. R. Lu, *Journal of The Royal Society Interface*, 2009, **6**, S659-S670.
34.   J. Penfold and R. Thomas, *Journal of Physics: Condensed Matter*, 1990, **2**, 1369.
35.   J. R. Lu, S. Perumal, E. T. Powers, J. W. Kelly, J. R. Webster and J. Penfold, *Journal of the American Chemical Society*, 2003, **125**, 3751-3757.
36.   B. J. Berne and R. Pecora, *Dynamic light scattering: with applications to chemistry, biology, and physics*, Courier Dover Publications, 2000.
37.   Z. Li, J. Lu and R. Thomas, *Langmuir*, 1997, **13**, 3681-3685.
38.   J. R. Lu, S. Perumal, X. Zhao, F. Miano, V. Enea, R. R. Heenan and J. Penfold, *Langmuir*, 2005, **21**, 3354-3361.
39.   W. F. Reed, S. Ghosh, G. Medjahdi and J. Francois, *Macromolecules*, 1991, **24**, 6189-6198.
40.   R. A. McAloney, M. Sinyor, V. Dudnik and M. C. Goh, *Langmuir*, 2001, **17**, 6655-6663.
41.   S. T. Dubas and J. B. Schlenoff, *Langmuir*, 2001, **17**, 7725-7727.

ToC

Intermediate filament-like aggregation from keratin polypeptides upon increasing [NaCl] as revealed by SANS